JOURNAL OF COMPUTATIONAL PHYSICS 77, 85–108 (1988)

A Computational Model of Aquatic Animal Locomotion

LISA J. FAUCI

Department of Mathematics, Tulane University, New Orleans, Louisiana 70118

AND

CHARLES S. PESKIN

Courant Institute of Mathematical Sciences, New York, New York 10012

Received April 17, 1987; revised July 8, 1987

A computational model of the swimming of a neutrally buoyant organism undergoing deformations within a region of fluid is presented. The fluid is regarded as viscous and incompressible and the organism as a massless, elastic boundary immersed in this fluid. Fluid quantities are represented on a grid (Eulerian description), and the immersed boundary is represented by a discrete collection of moving points (Lagrangian description). Computed results are presented, along with comparisons with previous asymptotic analysis.

1. INTRODUCTION

The principal means of aquatic animal locomotion is to pass waves of lateral displacement down the body. This mode of swimming is observed in large creatures such as eels, moderate size nematodes (thread worms), and microorganisms with flagella such as spermatozoa. The forces involved in the propulsion of these organisms are very different; in the first case, inertial effects dominate, in the last viscous effects dominate, and in the second both are comparable. An important distinction between these flows is the Reynolds number, a non-dimensional quantity which describes the ratio of inertial forces to viscous forces, given by

$$R = \frac{LU}{\nu},$$

where L is a typical length, U a typical velocity, and ν is the kinematic viscosity μ/ρ. The Reynolds number of a swimming eel is about 10^4, the nematode's about 1, and that of a spermatozoa about 10^{-3}. For an interesting and extensive classification of Reynolds numbers and swimming modes of different aquatic animals, we refer the reader to Lighthill [1] and Childress [2].

The speed, direction, and efficiency of swimming depend upon many parameters

0021-9991/88 $3.00

including the Reynolds number and the wavelength, amplitude, and frequency of undulation. We would like to know how the overall swimming speed of the organism relates to the speed of the wave, and how much energy is dissipated in the swimming effort.

In this paper we present a computational model of swimming of a neutrally buoyant organism undergoing deformations within a region filled with fluid. The fluid and the organism constitute a coupled mechanical system; the organism's motion is determined by that of the fluid, but at the same time the organism exerts force on the fluid and alters its motion.

The fluid is regarded as viscous and incompressible, and the organism as a massless, elastic boundary immersed in this fluid. The state of the fluid at time t is given by its velocity field $\mathbf{u}(\mathbf{x}, t)$, and the state of the organism is given by the configuration of its material points $\mathbf{X}(s, t)$, where s is an arc-length parameter. The flow is governed by the incompressible Navier–Stokes equations

$$\rho\left[\frac{\partial \mathbf{u}}{\partial t} + \mathbf{u}\cdot\nabla\mathbf{u}\right] = -\nabla p + \mu\Delta\mathbf{u} + \mathbf{F}(\mathbf{x}, t)$$

$$\nabla\cdot\mathbf{u} = 0$$

where ρ = density, μ = viscosity, $\mathbf{u}$ = velocity, p = pressure, and $\mathbf{F}(\mathbf{x}, t)$ is the external force per unit volume applied to the fluid.

The first equation is Newton's law: mass density × acceleration = force density. The second states that the fluid is incompressible. The forces which appear are those due to pressure, viscosity, and the external force $\mathbf{F}(\mathbf{x}, t)$. The external force will be used in this work to represent the force of the organism on the fluid. It is a delta-function layer of force supported only by the region of fluid which coincides with material points of the organism; away from these points the external force is zero. Since the organism is elastic and massless, the strength of the delta-function force layer is determined at each instant by the local configuration of the organism. Representing the immersed swimming organism as a singular force field in the fluid domain will be the basis of the computational model.

The boundary condition to be satisfied at the surface $\mathbf{X}(s, t)$ defined by the organism is

$$\frac{d}{dt}\mathbf{X}(s, t) = \mathbf{u}(\mathbf{X}(s, t), t).$$

This boundary condition states that the velocity of a point on the organism must be the same as the fluid velocity at that point.

The solution of the foregoing system of equations is difficult since the boundary will be undergoing time-dependent motions, and its position at any instant will depend upon the solution of the fluid equations, which are themselves nonlinear.

Previous theoretical work in this area has been limited to simplified versions of the fluid equations or asymptotic analysis. For example, the classic work of G. I.

Taylor [3] analyzes the swimming of an infinitely long flagella undergoing infinitely small, constant amplitude oscillations in a totally viscous fluid. This work was later extended by E. O. Tuck [4] to account for non-zero Reynolds numbers. In Section 7 of this paper we compare the results of our numerical studies to the asymptotic results of Taylor and Tuck.

The computational method presented in this paper solves the full Navier–Stokes equations in a two-dimensional domain of fluid in which an organism undergoing time-dependent motions is immersed. The organism consists of a single filament. No restriction is imposed on the size or position-dependence of the amplitude of oscillation, nor on the Reynolds number of the flow. We do not rely on the fact that the motion has reached a steady state, and we are therefore able to model transient effects. To our knowledge, this is the first computational method which makes these claims.

2. Representation of Fluid and Organism

We cover our fluid domain with a square grid on which we define the fluid quantities at grid points: $\mathbf{u}_{ij}^n = \mathbf{u}(i\,\Delta x, j\,\Delta x, n\,\Delta t)$, p_{ij}^n, and $\mathbf{F}_{ij}^n$, where $i, j = 1, 2, 3, \ldots, N$. The swimming organism is modeled by an immersed boundary $\mathbf{X}(s, t)$ which is discretely represented by a collection of M moving points $\mathbf{X}_k^n$, $k = 1, 2, \ldots, M$. The points do not coincide with grid points.

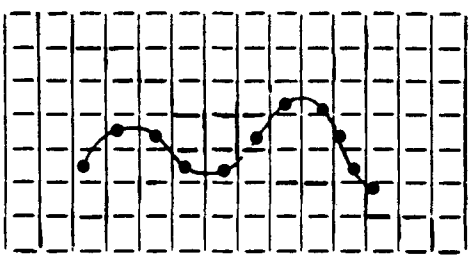

Ω

We use the external force $\mathbf{F}$ to represent the force of the organism on the fluid. $\mathbf{F}$ must be singular because the immersed boundary exerts a finite force in zero volume of the fluid. Hence, $\mathbf{F}$ is a distribution,

$$\mathbf{F}(\mathbf{x}, t) = \int_B \mathbf{f}(s, t)\, \delta(\mathbf{x} - \mathbf{X}(s, t))\, ds, \tag{2.2}$$

where δ is the two-dimensional delta function and $\mathbf{f}(s, t)$ is the density of the boundary force with respect to the measure ds. The boundary is considered to be elastic and massless so the force $\mathbf{f}(s, t)$ is determined by the boundary configuration at time t. (The derivation of $\mathbf{f}$ will be discussed later.) Note that despite the integral

representation, $\mathbf{F}(\mathbf{x}, t)$ is singular since we are integrating the two-dimensional delta function over only one dimension.

Since the fluid is viscous, the velocity field is continuous across the boundary. This implies that the velocity of a material point of the organism must be equal to the velocity of the fluid at that point:

$$\frac{\partial \mathbf{X}}{\partial t} = \mathbf{u}(\mathbf{X}(s, t), t) = \int_{\Omega} \mathbf{u}(\mathbf{x}, t)\, \delta(\mathbf{x} - \mathbf{X}(s, t))\, d\mathbf{x}. \tag{2.3}$$

The integral representation of $\partial \mathbf{X}/\partial t$ in (2.3) is not singular since the two-dimensional delta function is integrated over both space dimensions.

The integral equations (2.2) and (2.3) serve to communicate boundary quantities to the grid and fluid quantities to the boundary. These integrals can be discretized as sums,

$$\mathbf{F}_{ij}^n = \sum_k \mathbf{f}_k^n\, D_{ij}(\mathbf{X}_k)\, \Delta s \tag{2.2*}$$

$$\mathbf{U}_k^n = \sum_{ij} \mathbf{u}_{ij}^n\, D_{ij}(\mathbf{X}_k)\, \Delta x^2, \tag{2.3*}$$

where D_{ij} is the discrete approximation to the two-dimensional delta function introduced by Peskin [5]. D_{ij} serves the dual purpose of spreading the boundary force to the fluid mesh and interpolating the fluid velocity to boundary points.

Once $\mathbf{F}_{ij}$ has been defined, we can update the fluid quantities by calling a subroutine which integrates the Navier–Stokes equations for one-time step on a regular grid. The crucial point here is that this subroutine *does not see the immersed boundary at all* except in terms of the force field $\mathbf{F}_{ij}$.

Our immersed boundary is *not* the computational boundary in the Navier–Stokes solver, but a singular force field which alters the equation just via the right-hand side. There is no need for complicated discretization of derivatives at grid points near the organism or for boundary conditions which change with time. We can model complicated motions with a Navier–Stokes solver designed for a regular mesh with simple boundary conditions. For this purpose we use Chorin's finite difference scheme on a square, periodic grid. [6]

3. Derivation of Force Density

The immersed boundary, which is made up of the discrete set of points $\mathbf{X}_1, \mathbf{X}_2, \ldots, \mathbf{X}_M$ is elastic and massless. The forces at a point due to the rest of the boundary are of two types:

(1) A spring-like force that asks that the "links" between successive points resist compression or expansion from a given arc-length Δs.

(2) A bending-resistant force that asks that the angle formed by neighboring links be a given function which changes with position and time.

Since the boundary is massless, Newton's laws tell us that at a boundary point we have

> 0 = Mass × acceleration = Force of fluid on boundary point + Force of the rest of the boundary on boundary point

Therefore,

— Force of fluid on boundary point = Force of the rest of the boundary on boundary point.

And we have

> Force of boundary point on fluid = Force of the rest of the boundary on boundary point.

The swimming motion, that we will specify, is the time-dependent configuration of the organism *relative to itself*. The actual displacement and swimming speed relative to the grid are not preset, but are determined by the coupled equations of motion.

To impose (approximately) a given swimming motion on the immersed boundary, we use forces that are derived from a time-dependent energy function which depends upon the configuration of consecutive triples of points along the boundary. A way to guarantee that momentum and angular momentum are conserved is to choose an energy function $E(\mathbf{X}_1, \mathbf{X}_2, ..., \mathbf{X}_M, t)$ that is invariant under translation and rotation. This invariance further emphasizes the fact that the forces will only specify the *relative* configuration of the organism.

The force acting on the point $\mathbf{X}_k$ is equal to the negative of the derivative of the energy function with respect to $\mathbf{X}_k$:

$$\mathbf{f}_k = -\partial_k E = -\left[\frac{\partial E}{\partial x_k}, \frac{\partial E}{\partial y_k}\right].$$

$E(\mathbf{X}_1, \mathbf{X}_2, ..., \mathbf{X}_M, t)$ is chosen such that $E \geqslant 0$ and that $E = 0$ when the boundary configuration at time t is as desired.

We want to specify the arc length between points and the angle formed at each point:

$$E(\mathbf{X}_1, \mathbf{X}_2, ..., \mathbf{X}_M, t) = S_1 \sum_k [\|\mathbf{X}_{k+1} - \mathbf{X}_k\| - \Delta s]^2$$

$$+ S_2 \sum_k [\hat{z} \cdot (\mathbf{X}_{k+1} - \mathbf{X}_k) \times (\mathbf{X}_k - \mathbf{X}_{k-1}) - C_k(t)]^2.$$

(Here $\|\cdot\|$ is the Euclidean norm and $\hat{z}$ is the unit vector $(0, 0, 1)$.)

Now this is zero when the distance between successive points is Δs and the "curvature" at a point $\mathbf{X}_k$ is $C_k(t)$. We use the cross product instead of $\|d^2y/dx^2\|$ since it is important to specify the sense of the angle as well as its magnitude. When $E=0$, $C_k(t)$ is approximately equal to $\Delta s^3(d^2y/dx^2)$ as will be shown in the next section. The function $C_k(t)$ is what establishes the time dependence of the swimming motion.

S_1 and S_2 are stiffness constants which depend upon the arc-length interval Δs and determine how strictly the constraints are enforced. We may view the role of the stiffness constants in two ways:

(1) Physiological parameters. The creature's muscular structure will tend to generate a predetermined swimming motion but the effect of the fluid can alter this motion; how much alteration depends on the size of S_1 and S_2.

(2) Numerical parameters. The swimming motion of the creature (relative to itself) is completely specified in advance. Then S_1 and S_2 are both infinity. Computationally, they should be made as large as possible. (Penalty method.)

The above energy function can be adjusted to enforce many different configurations, but we concentrate on those of the form $y=a(x)\sin(\kappa x-\omega t)$, where $a(x)$ adjusts the variation of amplitude from head to tail. Appropriate values of $C_k(t)$ and the stiffness constants S_1 and S_2 will be discussed in the next section.

4. Derivation of the Driving Function $C_k(t)$

The function $C_k(t)$ is what establishes the shape and the time dependence of the swimming motion. The angles between successive links of length Δs at time t will be specified by

$$\begin{aligned} C_k(t) &= \hat{z}\cdot(\mathbf{X}_{k+1}-\mathbf{X}_k)\times(\mathbf{X}_k-\mathbf{X}_{k-1}) \\ &\approx (\Delta s)^2 \sin \Psi_k, \end{aligned}$$

where Ψ_k is the exterior angle formed by the links $(\mathbf{X}_{K+1}, \mathbf{X}_k)$ and $(\mathbf{X}_k, \mathbf{X}_{k-1})$. Note that this interpretation assumes that the arc-length constraint is working and hence that

$$\|\mathbf{X}_{k+1}-\mathbf{X}_k\| \approx \|\mathbf{X}_k-\mathbf{X}_{k-1}\| \approx \Delta s.$$

Given a curve $(x(s), y(s))$ parameterized by arc-length s, let $\Theta(s)$ be the angle formed by the tangent to the curve and the horizontal axis. In our discrete case, we let Θ_k be the angle formed by the link $(\mathbf{X}_{k-1}, \mathbf{X}_k)$ and the horizontal axis. We then have

$$\theta_{k+1}-\theta_k = d\theta_k = \Psi_k.$$

Substituting into the above equation for $C_k(t)$, we have

$$C_k(t) = (\Delta s)^2 \sin \Psi_k = (\Delta s)^2 \sin d\Theta_k.$$

Assuming that the links model a continuous curve, we have $d\theta_k \ll 1$, and we make the approximation

$$\sin d\theta_k \approx d\theta_k$$

which gives us

$$C_k(t) \approx (\Delta s)^2 \, d\theta_k \approx (\Delta s)^3 \frac{d\theta_k}{ds}.$$

The continuous variable corresponding to $C_k(t)/(\Delta s)^3$ is $c(s, t) = \partial\theta/\partial s$, which is called the *curvature*. Note that the configuration of the creature relative to itself (i.e., the shape) is completely determined by specifying the curvature. The differential equations needed to compute $(x(s, t), y(s, t))$ from $c(s, t)$ are

$$\frac{\partial\theta}{\partial s} = c(s, t)$$

$$\frac{\partial x}{\partial s} = \cos\theta(s, t)$$

$$\frac{\partial y}{\partial s} = \sin\theta(s, t).$$

The integration constant in the θ equation determines the orientation of the creature, and the integration constants in the (x, y) equations determine its absolute position in space.

For comparison with asymptotic theories, we seek a one-parameter family of curvature functions chosen so that the small amplitude configuration of the creature will be

$$x(s, t) = x_0(t) + s + O(\varepsilon^2)$$
$$y(s, t) = \varepsilon y_1(s, t) + O(\varepsilon^2),$$

where

$$y_1(s, t) = a(s) \sin(\kappa s - \omega t).$$

It follows that

$$\theta(s, t) = \varepsilon\theta_1(s, t) + O(\varepsilon^2)$$
$$c(s, t) = \varepsilon c_1(s, t) + O(\varepsilon^2),$$

where

$$c_1(s, t) = \frac{\partial \theta_1}{\partial s} = \frac{\partial^2 y_1}{\partial s^2}$$

$$= \left(\frac{\partial^2 a}{\partial s^2} - \kappa^2 a(s) \right) \sin(\kappa s - \omega t) + 2\kappa \frac{\partial a}{\partial s} \cos(\kappa s - \omega t).$$

In the special case $a = \text{constant}$, this reduces to

$$c_1(s, t) = -\kappa^2 a \sin(\kappa s - \omega t).$$

In either case, we have

$$C_k(t) = \varepsilon(\Delta s)^3 c_1(s_k, t),$$

where

$$s_k = k \Delta s.$$

(In practice we set $\varepsilon = 1$ and achieve small amplitude, if desired, by adjusting a.) We shall use the above prescription for $C_k(t)$ even in the large-amplitude case. The resulting shape of the boundary will then be more complicated, however.

5. Stiffness Constants

For a fixed $\Delta s \neq 0$, the energy function was given as

$$E(\mathbf{X}_1, \mathbf{X}_2, ..., \mathbf{X}_M, t) = S_1 \sum_k [\|\mathbf{X}_{k+1} - \mathbf{X}_k\| - \Delta s]^2$$

$$+ S_2 \sum_k [\hat{z} \cdot (\mathbf{X}_{k+1} - \mathbf{X}_k) \times (\mathbf{X}_k - \mathbf{X}_{k-1}) - C_k(t)]^2.$$

The motion will tend to minimize this energy, but how strictly this is enforced depends upon the magnitude of the constants S_1 and S_2. S_1 and S_2 are independent of space and time, but, as we now show, they do depend upon the arc-length interval Δs.

We would like the energy function given above to reflect material properties of the elastic boundary which are independent of the arc-length Δs. We therefore require that the energy function E converge to a finite limit as $\Delta s \to 0$. Namely,

$$\tilde{E}(\mathbf{X}, t) = \tilde{S}_1 \int \left[\left\| \frac{d\mathbf{X}}{ds} \right\| - 1 \right]^2 ds + \tilde{S}_2 \int \left[\frac{d^2\mathbf{X}}{ds^2} \cdot \mathbf{n} - c(s, t) \right]^2 ds,$$

where the integration is over the continuous immersed boundary, $c(s, t)$ is the cur-

vature function introduced above, and $\mathbf{n}$ is the unit rightward-pointing normal to the curve.

By rewriting each of the finite sums in the original energy function $E(\mathbf{X}_1, \mathbf{X}_2, ..., \mathbf{X}_M, t)$ in the form of a Riemann sum, we find that in order for convergence to occur

$$S_1 = \tilde{S}_1(\Delta s)^{-1}$$
$$S_2 = \tilde{S}_2(\Delta s)^{-5},$$

where $\tilde{S}_1$ and $\tilde{S}_2$ are constant. It is important that the constants $\tilde{S}_1$ and $\tilde{S}_2$ be chosen large enough so that the desired configuration is closely held.

6. Numerical Method

The state of the coupled mechanical system at time t is determined by the velocity field of the fluid $\mathbf{u}(\mathbf{x}, t)$ and the positions of the material points of the immersed boundary $\mathbf{X}(s, t)$. Computationally, at the end of the nth time step, we are given $\mathbf{u}_{ij}^n$ and $\mathbf{X}_k^n$. From these we must advance another time step to produce $\mathbf{u}_{ij}^{n+1}$ and $\mathbf{X}_k^{n+1}$. The procedure is

(1) Determine the force density $\mathbf{f}_k^n$ defined on boundary points.

(2) Spread the force density to the grid to get $\mathbf{F}_{ij}^n$.

(3) Solve the Navier–Stokes equations for $\mathbf{u}_{ij}^{n+1}$.

(4) Interpolate the fluid velocity field to boundary points and move the boundary at this local fluid velocity:

$$\mathbf{X}_k^{n+1} = \mathbf{X}_k^n + \Delta t\, \mathbf{U}_k^{n+1}.$$

Step (1) is the "boundary segment" of the code, and it entails solving an unconstrained minimization problem at each time step. This enhances the numerical stability of the method, as explained in Peskin [5]. For this minimization, we use a modified Newton's method outlined in Dennis and Schnabel [7]. Step (3) is the fluid segment of the code, which uses Chorin's finite difference scheme [6]. The Poisson equation for the pressure field which arises is solved using a fast Fourier transform. Steps (2) and (4) involve the use of the discrete delta functions, which serve the purpose of "communicating" information between the boundary and the fluid.

This code has been implemented on Boeing's CRAY XMP and the Minnesota Supercomputer Center's CRAY 2. Using a 64×64 grid, the fluid segment of the code (step (3)) requires, on the average, 0.02 s CPU time, the force segment (step (1)) requires 0.09 s, and the delta function segment (steps (2) and (4)) requires 0.04 s. Therefore, one time step requires about 0.15 s CPU time on the

CRAY XMP. (The timings on the CRAY 2 were almost identical.) These timings reflect the fact that the fluid segment of the code has been completely vectorized.

For detailed explanation of the implementation of these algorithms, see Fauci [8].

7. Swimming Sheet Problem

In this section we apply our computational model to the infinite swimming sheet problem. We compare our results with the asymptotic analysis done for small amplitude motion by Taylor [3] and Tuck [4].

This problem involves the swimming of a doubly infinite sheet, which undergoes periodic deformations about an unperturbed position $y=0$. The sheet oscillates with a constant amplitude, wavelength, and frequency. It is surrounded by a viscous fluid on both sides. For a given amplitude, wavelength, and frequency of motion, we would like to know the speed at which the sheet propels itself through the fluid and how much energy is dissipated.

A two-dimensional slice of the sheet is of the form

$$y = b \sin(\kappa x - \omega t)$$

with respect to "axes which are fixed relative to the mean position of the particles of the sheet" [3]. This shall be referred to as the organism's frame of reference.

The above sine wave travels to the right with phase speed $V=\omega/\kappa$ and period $2\pi/\omega$. We let U be the resulting mean swimming speed of the sheet over a period. (The swimming speed is defined to be the mean speed of the fixed axes in the organism frame of reference relative to the axes fixed in the frame of reference where the fluid at infinity is undisturbed.) It is important to note that U is not given, but will be determined by the fluid equations. A useful, non-dimensional quantity to study is the ratio of swimming speed to wave speed U/V. This ratio also measures

$$\frac{U}{V} = \frac{\text{number of wavelengths travelled}}{\text{period}}.$$

G. I. Taylor considered the case of zero Reynolds number flow, where the forces due to viscosity completely dominate those due to inertia. This is a very reasonable assumption for the study of propulsion of microorganisms, where the Reynolds number is typically $O(10^{-4})$. This assumption greatly simplifies the governing fluid equations; the nonlinear convection term is dropped.

Assuming that the sheet is inextensible, and using the non-dimensional scaling $\kappa = 1$ for simplicity, Taylor arrived at

$$u_s = \frac{\omega}{4} b^2 \cos 2(x - \omega t) + O(b^4)$$

$$v_s = -\omega b \cos(x - \omega t) + O(b^3).$$

Here (u_s, v_s) is the velocity vector of the boundary point (x_s, y_s), and x is the mean position of x_s in the organism frame of reference. Notice that if only terms up to order b are retained

$$u_s = 0$$
$$v_s = -\omega b \cos(x - \omega t).$$

The particles oscillate in a path parallel to the y-axis.

However, retaining those powers up to b^2 and integrating, we have

$$x_s = x - \tfrac{1}{8} b^2 \sin 2(x - \omega t)$$
$$y_s = b \sin(x - \omega t).$$

The particles traverse paths of figure eights. This will be observed in our case studies of the next sections.

Using an asymptotic expansion of the stream function, Taylor concluded

$$\frac{U}{\omega} = \frac{1}{2} b^2 \left(1 - \frac{19}{16} b^2\right) + O(b^6)$$

and for arbitrary κ,

$$\frac{U}{V} = \frac{1}{2} b^2 \kappa^2 \left(1 - \frac{19}{16} b^2 \kappa^2\right) + O(b^6 \kappa^6).$$

Up to first order in b, the sheet does not swim!

The dissipation of energy can be computed by calculating the work done per unit area of the sheet against the viscous stress. The mean value (over a period $2\pi/\omega$) of the rate of working was calculated by Taylor to be

$$W = 2b^2 \omega^2 \kappa \mu,$$

where μ is the viscosity of the fluid. Here, the expansion only up to $O(b\kappa)$ was used.

Taylor's calculations are designed for small amplitude motion, and zero Reynolds number flow. In his paper of 1968, E. O. Tuck analyzed the case of small amplitude motion taking inertia into account.

The Reynolds number defined for the swimming sheet problem is

$$R = \frac{\omega}{\nu \kappa^2},$$

where $\nu = \mu/\rho$ is the kinematic viscosity, ω/κ is a typical velocity, and $1/\kappa$ is a typical length. Tuck found that

$$\frac{U}{V}=\frac{1}{4}b^2\kappa^2\left[1+\frac{1}{F(R)}\right]+O(b^4\kappa^4)$$

$$F(R)=\left[\frac{1+\sqrt{1+R^2}}{2}\right]^{1/2}.$$

The mean rate of working as calculated by Tuck is

$$W=\mu b^2\omega^2\kappa(1+F(R)).$$

Note that for $R=0$, the above reduces to Taylor's expression for W.

Computational Studies

In order to model the infinite swimming sheet, we let the computational domain be a square whose side equals one wavelength of the sheet. The immersed boundary extends from one end of the domain to the other. The periodicity condition will simulate the infinite extent of the sheet. (We could have explicitly linked the first and last point of the immersed boundary by coupling these points in the energy function, with minor changes to the code. Ultimately, however, our goal is to model organisms of finite extent.) The velocity field is initialized to zero.

In the parameter studies I and II, the values in Table I were fixed, but the amplitude of oscillation was varied. As shown in Table I, the Reynolds number in study I is approximately 2.5, and in study II it is approximately 0.6. The Reynolds number, based on wavelength, is calculated as

$$R=\frac{\rho\omega}{\mu\kappa^2}.$$

The calculations were performed on a 64×64 grid with 128 points comprising the immersed boundary. In each of the numerical experiments, the code was run until a (periodic) steady state was reached, which took at most five periods. The swimming velocity U was arrived at by first averaging the x-direction velocity of each boundary point over a period and then taking the average of these values over all points of the creature.

TABLE I

Parameter Studies

Parameter	Symbol	Units	I	II
Wave no.	κ	cm^{-1}	10π	10π
Frequency	ω	s^{-1}	8π	8π
Density	ρ	gm/cm^3	1	1
Viscosity	μ	gm/cm s	0.01	0.04
Reynolds no.	R	—	2.5	0.6

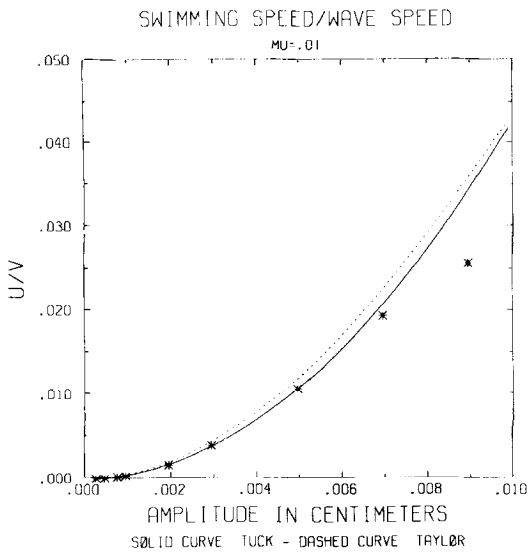

FIG. 1. Parameter study I. Computed values of U/V for various amplitudes are plotted against Taylor's formula (dashed curve) and Tuck's formula (solid curve), $R \approx 2.5$.

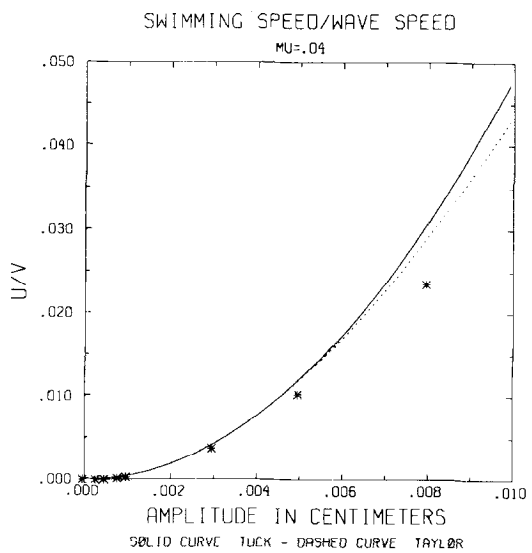

FIG. 2. Parameter study II. Computed values of U/V for various amplitudes are plotted against Taylor's formula (dashed curve) and Tuck's formula (solid curve), $R \approx 0.6$.

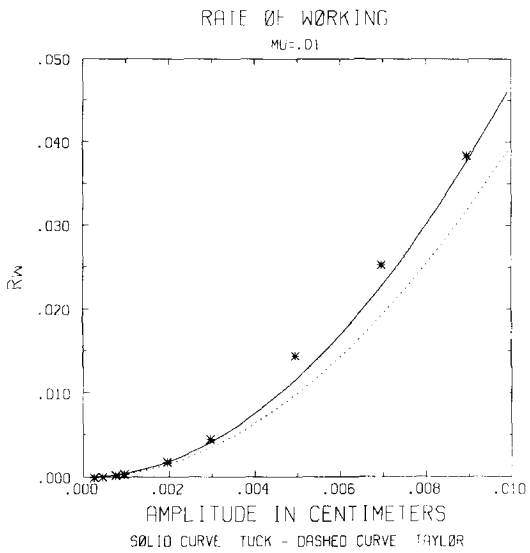

FIG. 3. Parameter Study I. Computed values of mean rate of working for various amplitudes are plotted against Taylor's formula (dashed curve) and Tuck's formula (solid curve), $R \approx 2.5$.

Figure 1 compares the results of parameter study I ($R \approx 2.5$) with the asymptotic formulas for U/V of Taylor (dashed curve) and Tuck (solid curve). The *'s indicate the computed values U/V for different amplitude values. Notice that both Taylor's and Tuck's asymptotic predictions are better for smaller amplitudes, as expected. However, Tuck's formula, which takes inertia into account, fits the computed values better than Taylor's formula.

Figure 2 shows the results from parameter study II. Here Taylor's approximations for the larger amplitudes are a bit better than Tuck's since the Reynolds number is closer to zero, and Taylor's asymptotic analysis was carried out to $O(b^4\kappa^4)$, whereas Tuck's was carried out to $O(b^2\kappa^2)$. (Here b is the amplitude of motion.)

results were obtained in parameter study II.

Our computations indicate that the asymptotic analysis overestimates the swimming speeds, and underestimates the rate of working. We see that the analysis of Taylor and Tuck is sufficient for small amplitude and slope oscillations, but other methods, such as this computational model, must be used to study larger amplitude propulsion.

8. Case Studies

In this section we conduct two case studies of swimming of an oscillating filament. In these two cases, we shall choose an energy function which will tend to impose constant amplitude from head to tail. However, the method does not restrict us to this constant amplitude situation.

For both cases the energy function is chosen so that the time-dependent configuration of the organism relative to itself is of the form

$$x \approx s$$

$$y \approx b \sin(\kappa s - \omega t).$$

The Reynolds number of the flow is given by

$$R = \frac{\omega}{\nu \kappa^2},$$

where $\nu = \mu/\rho$ is the kinematic viscosity.

We set density at $\rho = 1\ \text{gm/cm}^3$, viscosity $\mu = 0.01\ \text{gm/(s} \cdot \text{cm)}$, $\omega = 8\pi\ \text{s}^{-1}$, and $\kappa = 10\pi\ \text{cm}^{-1}$. Therefore, the Reynolds number is

$$R \approx 2.5.$$

In this first case study, the amplitude of the waving motion is very small; 1% of the wavelength. In the second case, we study a more substantial amplitude of motion, which is 10% of the wavelength.

8.1. *Small Amplitude Case*

The following numerical experiment was performed on the CRAY-2 at the Minnesota Supercomputer Center, using a 64×64 grid, with 128 points constituting the immersed boundary. Periodic boundary conditions were imposed. The sine wave parameters κ and ω were set at the above values, and the amplitude was taken to be

$$b = 0.002\ \text{cm}.$$

The length of a side of the square computational domain is 0.2 cm, which is equal to one wavelength of the filament. Our reason for setting up the computation in this manner is to compare our results with the asymptotic analysis done for the *infinite* swimming sheet problem, which was presented in the previous section. With 64 grid points in each direction, we have

$$\Delta x = \frac{0.2}{64}\ \text{cm} = 0.003125\ \text{cm}.$$

One special feature of the computational method is its ability to handle sub-grid

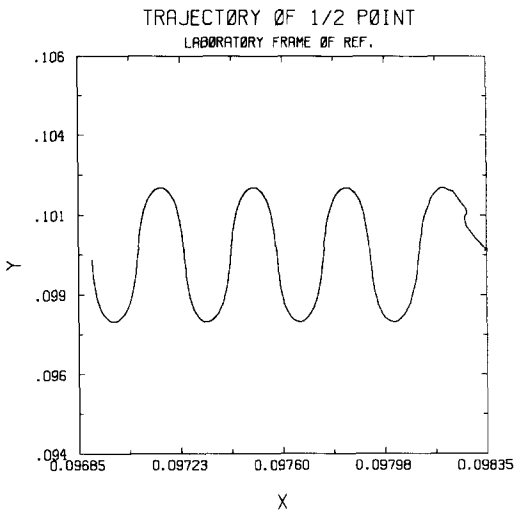

FIG. 4. Trajectory of the material point $\mathbf{X}_{64}$ from $t=0$ to $t=1$ s in the small amplitude case $b=0.002$ cm. The curve was traversed from right to left.

motion. The material points of the immersed boundary do not coincide with grid points. In this particular case, the amplitude of the wave is less than two-thirds of the mesh spacing.

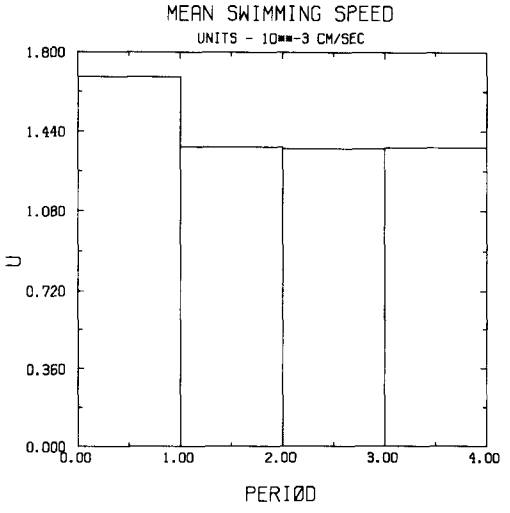

FIG. 5. The mean swimming speed averaged over each of the four periods. Note the acceleration from rest in the first period, and then the establishment of a steady periodic state.

The particles of the immersed boundary are initialized to lie along the specified sine wave, with centerline corresponding to the center of the computational domain. The particles extend from one side of the domain to the other. The arc-length parameter used is

$$\Delta s = \tfrac{1}{2}\,\Delta x = 0.0015225 \text{ cm}.$$

The stiffness parameters used are

$$S_1 = 10{,}000(\Delta s)^{-1}$$
$$S_2 = 10\,(\Delta s)^{-5}.$$

The fluid velocities are initialized to zero.

The phase speed of the sine wave is 0.8 cm/s, and the period of motion is 0.25 s. Using $\Delta t = 0.00025$ s, we ran the code for 4000 time steps, four periods, up to $t = 1$ s.

Figure 4 shows the particle trajectory of the point $\mathbf{X}_{64}$. These curves were traversed from right to left as time progressed from $t = 0$ to $t = 1$ s. After some acceleration and irregularity in the first period, we see that the trajectories have settled into a steady, periodic motion.

The mean swimming velocity of the organism is computed by averaging the x-direction velocity of each point over a period, and then taking the average of these.

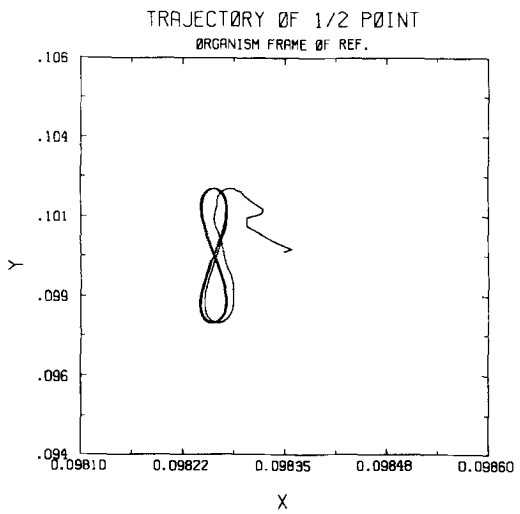

FIG. 6. In the frame of reference moving with the organism, trajectory of the material $\mathbf{X}_{64}$ from $t = 0$ to $t = 1$ s in the small amplitude case $b = 0.002$ cm.

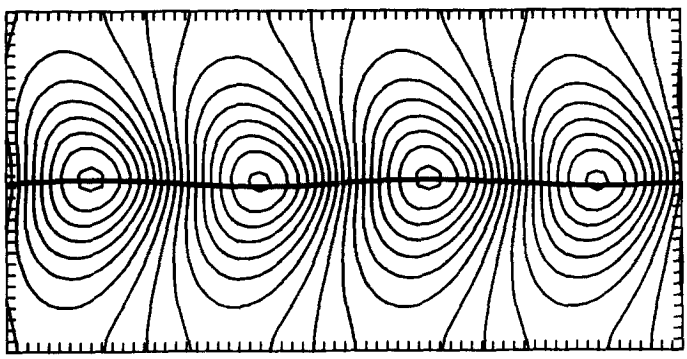

FIG. 7. Position of filament and streamlines of velocity field at $t = 1$ s. Dimensions of rectangle are 0.4 cm × 0.2 cm.

Figure 5 shows the mean swimming speed in each of the four periods. Note the acceleration from rest in the first period, and then the establishment of a steady swimming speed.

As was discussed in the previous section, G. I. Taylor [3] discovered that for small amplitude motion, the material points of the waving filament will traverse paths of narrow figure eights in the frame of reference moving with the organism. Since we have calculated the mean swimming velocity U, we re-plot the material point trajectory of Fig. 4 in this frame of reference

$$x' = x - Ut$$

$$y' = y$$

$$t' = t.$$

This is shown in Fig. 6.

The progress made in the direction of swimming after one second in this small

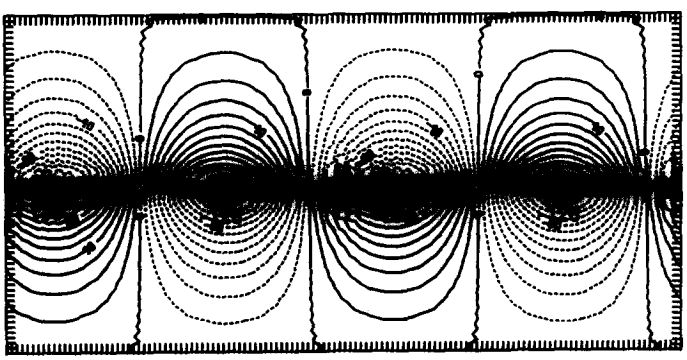

FIG. 8. Pressure contours at $t = 1$ s.

amplitude case is less than one-half of one mesh spacing. We therefore do not show successive snapshots of the motion in time. Figure 7 shows the streamlines of the velocity field with the immersed boundary at $t = 1$ s. Figure 8 shows the pressure contours of the fluid at $t = 1$ s. Since periodic boundary conditions were used, both Figs. 7 and 8 are comprised of two domains placed side by side. The pressure gradient is supported mainly by the immersed boundary. Therefore, near this boundary, which appears to the fluid grid as a straight line, there are many contour levels. The dark line in the center of the contour plot was *not* explicitly drawn in, but put there by the contour-drawing package.

We have checked to see how closely the constraints imposed by the energy function were enforced by the configuration of points after 4000 time steps at $t = 1$. The average relative error in arc length

$$\frac{1}{M-1}\sum_{k=1}^{M-1}\left|\frac{\|\mathbf{X}_{k+1}-\mathbf{X}_k\|-\Delta s}{\Delta s}\right|$$

at $t = 1$ was computed to be 0.00017. The average relative error in adhering to the sine wave

$$\frac{1}{M}\sum_{k=1}^{M}\frac{|y_k-(0.1+0.002\sin((k-1)\,\Delta s^{*}\,10\pi-8\pi))|}{0.002}$$

at $t = 1$ was computed to be 0.014.

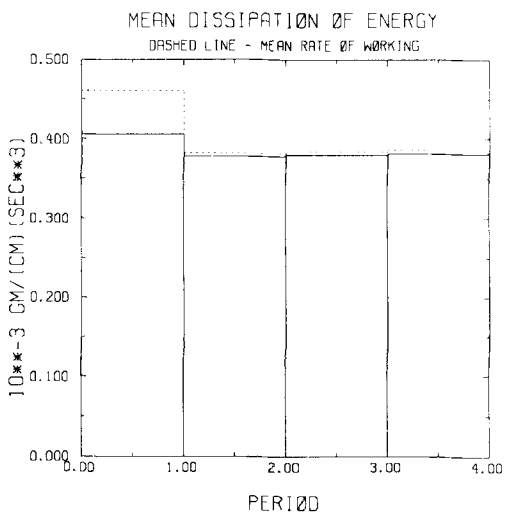

FIG. 9. The mean dissipation of energy and the mean rate of working averaged over each of the four periods. Once the system has reached a steady periodic state, apart from discretization error, the two should be equal.

The rate of working of the organism on the fluid is given by

$$\int \mathbf{f} \cdot \mathbf{U}\, ds,$$

where the integration is over the immersed boundary, $\mathbf{f}$ is the force density, and $\mathbf{U}$ is the velocity defined on the boundary.

The dissipation of energy in the fluid is given by

$$\frac{\mu}{2} \int \left(\frac{\partial u_i}{\partial x_j} + \frac{\partial u_j}{\partial x_i} \right)^2 d\mathbf{x},$$

where the integration is over the fluid domain, $\mathbf{u} = (u_1, u_2)$ is the fluid velocity field, and the summation convention is used.

The two integrals above are related by the energy identity

$$\frac{d}{dt}\left(\frac{\rho}{2} \int |\mathbf{u}|^2\, d\mathbf{x} \right) + \frac{\mu}{2} \int \left(\frac{\partial u_i}{\partial x_j} + \frac{\partial u_j}{\partial x_i} \right)^2 d\mathbf{x} = \int \mathbf{f} \cdot \mathbf{U}\, ds.$$

Assuming the motion has settled down to a periodic state, averaging each of the integrals in the above identity over a period tells us that the mean rate of working is equal to the mean dissipation of energy. (Over a period, the average rate of change of kinetic energy is zero.)

The integrals for the rate of working and the dissipation of energy are discretized into Riemann sums and computed at each time step. Each of these quantities is averaged over a period. This is a good check of the numerical method, since the integral for the rate of working involves boundary quantities, and the integral for the dissipation of energy involves fluid quantities. Figure 9 shows the mean dissipation of energy vs period and the mean rate of working vs period. Note that the two quantities differ appreciably after one period, since the motion had not reached an equilibrium: the mean rate of change of kinetic energy was not zero. However, after the motion has settled down, the two quantities are almost equal, the difference being due to discretization errors.

8.2. *Large Amplitude Case*

This numerical experiment is the same as the foregoing except that the amplitude of the swimming motion is ten times larger:

$$b = 0.02 \text{ cm}.$$

The time step used here is $\Delta t = 0.00005$ s (5 times smaller than above). We ran the code for 40,000 time steps, eight periods, up to $t = 2$ s.

Figures 10 and 11 show snapshots of the streamlines of the flow and the position of the organism during the first and eighth period of motion. Since the boundary

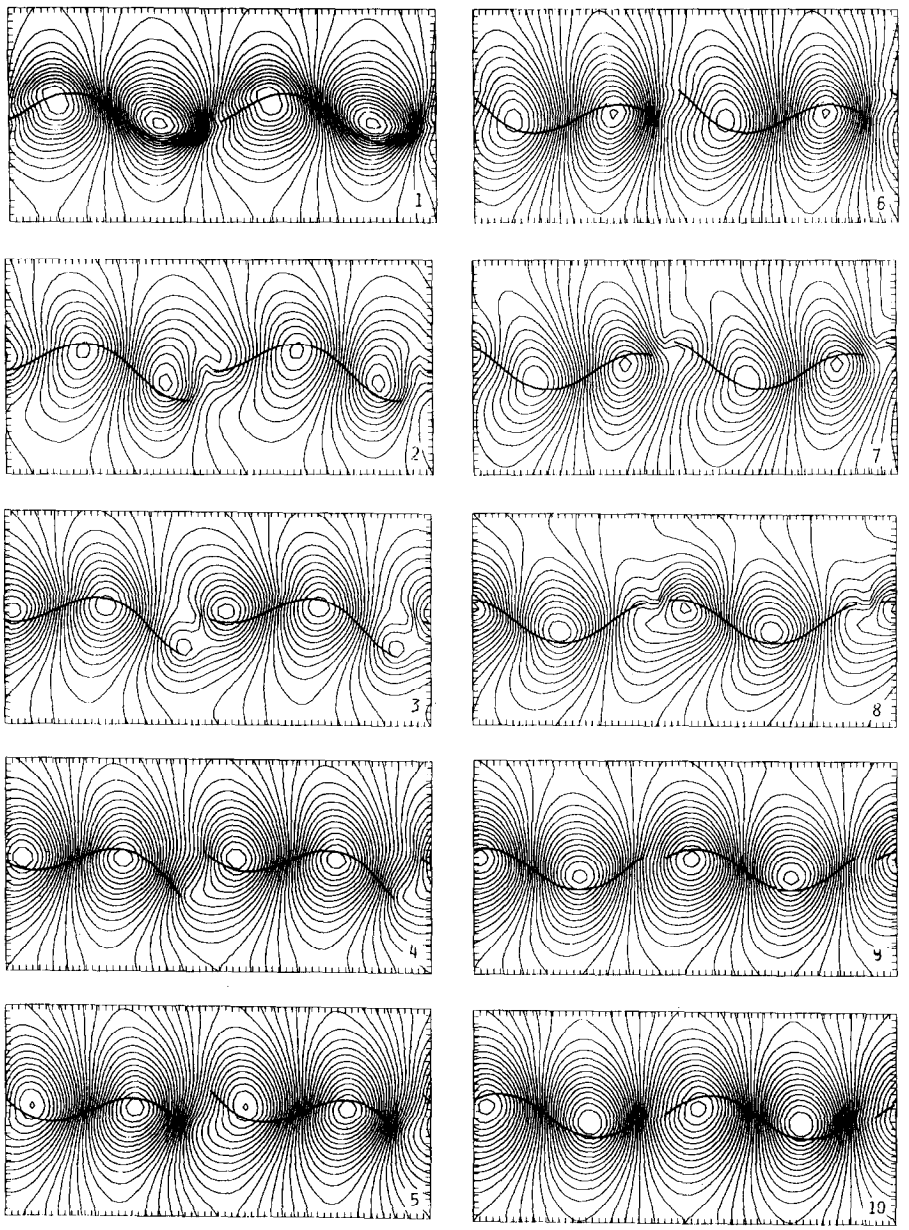

FIG. 10. Period 1. Snapshots of streamlines of flow field and position of filament at equally spaced time steps within the first period $t = 0$ to $t = 0.25$ s.

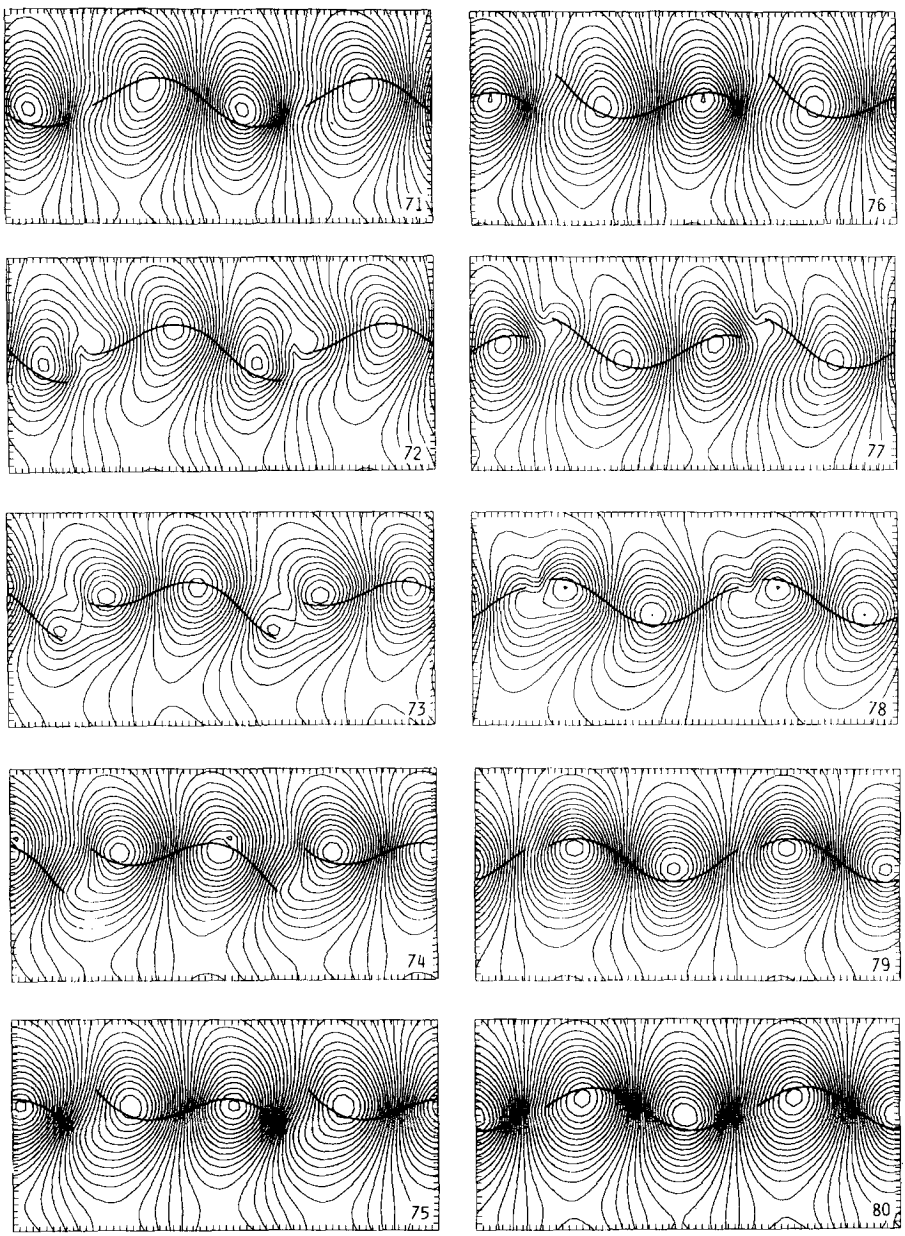

FIG. 11. Period 8. Snapshots of streamlines of flow field and position of filament at equally spaced time steps within the eighth period $t = 1.75$ to $t = 2$ s.

conditions are periodic, each snapshot is comprised of two domains. The wave goes over the filament from left to right, and the resulting swimming motion is to the left. Each figure contains ten graphs at equally spaced time intervals in the period. Note that as time progresses, the organism "leaves from the left and enters through the right."

Figure 12 shows snapshots of the streamlines of the velocity field and the pressure contour of the fluid at time $t = 0.00005$ s. Again, the position of the immersed boundary in the pressure contour was not explicitly drawn, but was provided by the routine which graphed the contour levels.

The desired configuration is not held as closely in this particular case as in the previous small amplitude case. The average relative error in arc length at $t = 1$ is 0.0054 and at $t = 2$ is 0.0053. The average relative error in adhering to the sine wave at $t = 1$ is 0.42, and at $t = 2$ is 0.85. The tail tends to move with larger amplitude than the rest of the body. Since the front of the filament faces drags, the tail is pushing forward and, hence, has the larger amplitude. If one seeks to enforce the constraints to a greater degree, the stiffness constants must be increased.

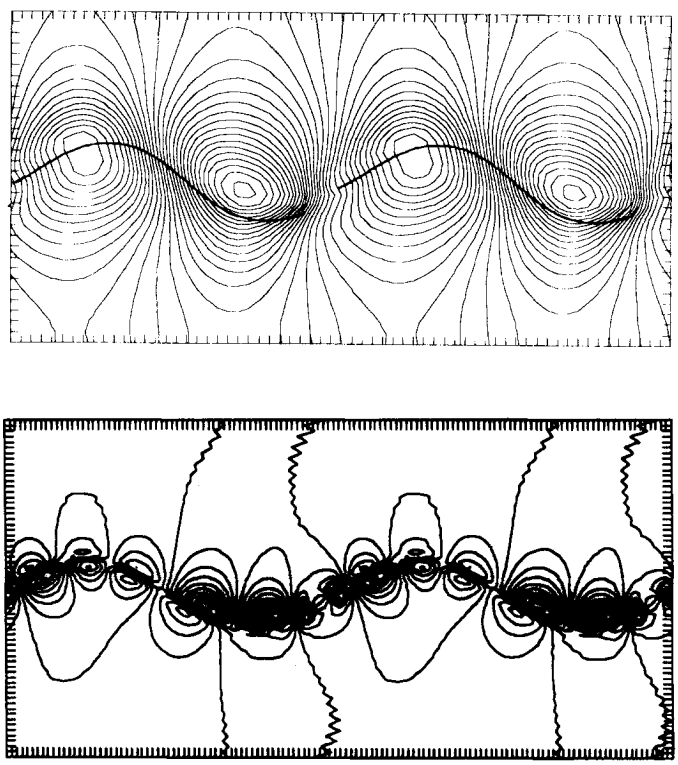

FIG. 12. Streamlines of velocity field and pressure contours at $t = 0.0005$ s. Dimensions of rectangles are 0.4 cm × 0.2 cm.

9. Conclusions

We have presented a new numerical model of aquatic animal locomotion, which has proven to be reliable in two dimensions. The results compare quite favorably with previous theoretical results, as shown in Section 7. However, the restrictive assumptions made in the asymptotic methods are not at all necessary in our model. The computational creatures need not be infinitely long and their swimming motions are not of infinitely small amplitude. Moreover, this computational model makes it possible to study more complicated motions such as a wave motion with an amplitude and/or a wavelength that varies from head to tail. In short, the computational approach makes it feasible to study models that are realistic enough to do justice to nature's complexity of design.

We are confident that this method will help answer many questions about the hydrodynamics of swimming. Within the scope of two dimensions, we are presently investigating the effect of variable amplitude on the efficiency of swimming, and the interaction of neighboring flagella (phase-locking). We hope to extend this model to three dimensions in the immediate future.

Acknowledgments

This work is supported in part by the National Science Foundation Grant DMS-8312229 and by the Mac Arthur Foundation.

References

1. J. L. Lighthill, *Mathematical Biofluiddynamics*, Regional Conference Series in Applied Mathematics (SIAM, Vol. 17, Philadelphia, PA, 1975).
2. S. Childress, *Mechanics of Swimming and Flying* (Cambridge Univ. Press, London, 1981).
3. G. I. Taylor, *Proc. R. Soc. Ser. A* **209**, 447 (1951).
4. E. O. Tuck, *J. Fluid Mech.* **31**, 305 (1968).
5. C. S. Peskin, *J. Comput. Phys.* **25**, 220 (1977).
6. A. J. Chorin, *Math. Comput.* **22**, 745 (1968).
7. J. E. Dennis and R. E. Schnabel, *Numerical Methods for Unconstrained Optimization and Nonlinear Equations* (Prentice–Hall, Englewood Cliffs, NJ, 1983).
8. L. Fauci, Thesis, Courant Institute of Mathematical Sciences, New York, NY, October, 1986 (unpublished).